Geophysical Research Letters

RESEARCH LETTER
10.1029/2023GL105796

Key Points:

- Analytical approximations of atmospheric temperature and surface albedo are used to estimate feedbacks in comprehensive climate models
- Meridional, seasonal, and global variations in feedbacks are well-represented by the analytical model, including in the polar regions
- Analytical feedbacks have less intermodel spread than general circulation model feedbacks, suggesting that deviations from an adiabat contribute to uncertainty

Supporting Information:

Supporting Information may be found in the online version of this article.

Correspondence to:

N. Feldl,
nfeldl@ucsc.edu

Citation:

Feldl, N., & Merlis, T. M. (2023). A semi-analytical model for water vapor, temperature, and surface-albedo feedbacks in comprehensive climate models. *Geophysical Research Letters*, *50*, e2023GL105796. https://doi.org/10.1029/2023GL105796

Received 3 AUG 2023
Accepted 3 OCT 2023

A Semi-Analytical Model for Water Vapor, Temperature, and Surface-Albedo Feedbacks in Comprehensive Climate Models

Nicole Feldl[1] and Timothy M. Merlis[2]

[1]Department of Earth and Planetary Sciences, University of California, Santa Cruz, Santa Cruz, CA, USA, [2]Program for Atmospheric and Oceanic Sciences, Princeton University, Princeton, NJ, USA

Abstract Radiative feedbacks govern the Earth's climate sensitivity and elucidate the geographic patterns of climate change in response to a carbon-dioxide forcing. We develop an analytical model for patterned radiative feedbacks that depends only on changes in local surface temperature. The analytical model combines well-known moist adiabatic theory with the radiative-advective equilibrium that describes the energy balance in high latitudes. Together with a classic analytical function for surface albedo, all of the non-cloud feedbacks are represented. The kernel-based analytical feedbacks reproduce the feedbacks diagnosed from global climate models at the global, zonal-mean, and seasonal scales, including in the polar regions, though with less intermodel spread. The analytical model thus provides a framework for a quantitative understanding of radiative feedbacks from simple physics, independent of the detailed atmospheric and cryospheric responses simulated by comprehensive climate models.

Plain Language Summary Given an increase in carbon dioxide concentration, individual radiative feedbacks stabilize or amplify the climate response. When diagnosed from comprehensive climate models, these feedbacks exhibit considerable variability, yet, single atmospheric columns have been successfully used as minimal models to quantify the effect of temperature and water vapor changes on global climate. Here, we bring together these perspectives by developing an analytical model for radiative feedbacks that, for projected changes, knows only of local surface temperature. That is, thermodynamic expressions for atmospheric temperature, water vapor, and sea-ice albedo are combined with radiative kernels, which characterize the top-of-atmosphere radiative response to a small perturbation, to yield estimates of radiative feedbacks independent of the simulated atmospheric and cryospheric changes from a climate model. The analytical model captures the equator-to-pole and seasonal feedback structure, including in the ice-covered polar regions, as well as the global feedback across an ensemble of global climate models. This research thus provides a framework for a quantitative understanding of radiative feedbacks from simple physics combined with geographic patterns of surface warming.

1. Introduction

The longwave clear-sky feedback is a key determinant of the Earth's climate sensitivity, representing the efficiency of atmospheric warming and moistening on the outgoing longwave radiation (OLR). Its magnitude has been constrained to -1.5 to -2 W m^{-2} K^{-1} for a wide range of surface temperatures and using both idealized (Koll & Cronin, 2018; McKim et al., 2021) and realistic (Chung et al., 2010; Dessler et al., 2008; Raghuraman et al., 2019; Raval & Ramanathan, 1989; Zelinka et al., 2020) atmospheric conditions. Recent physical explanations have centered on a spectral perspective of water vapor. According to Simpson's model, at wavelengths dominated by water vapor emission, OLR is insensitive to surface warming (Simpson, 1928). Thus, the observed linear dependence of OLR on surface temperature originates from the water vapor window and is equivalent to surface cooling to space (i.e., a surface Planck feedback) (Koll & Cronin, 2018). Implicit in this modified Simpson's model is a cancellation of atmospheric temperature and water vapor feedbacks (Ingram, 2010), which has been verified by line-by-line radiative transfer calculations (Jeevanjee et al., 2021), bolstering the case for feedback definitions centered on relative rather than specific humidity (Held & Shell, 2012). Yet, evidence from comprehensive general circulation models (GCMs) suggests these simple radiative arguments do not fully explain clear-sky feedbacks for realistic atmospheres. In particular, atmospheric cooling to space has been shown to account for large portions (up to 50%) of the clear-sky longwave feedback (Feng et al., 2023; Raghuraman et al., 2019). This discrepancy mandates extensions to the spectral feedback framework (Koll et al., 2023) or a shift beyond

a surface-Planck-dominant perspective to one that incorporates atmospheric influences on the increase in OLR with warming.

Multimodel comparisons conventionally diagnose the individual feedbacks (temperature, water vapor, etc.) that contribute to the net top-of-atmosphere radiative response to a carbon dioxide (CO_2) forcing. Local applications of feedback analysis (Feldl & Roe, 2013) have proven valuable for identifying the governing processes for the polar-amplified pattern of surface warming (Pithan & Mauritsen, 2014) and changes in atmospheric energy transport (Zelinka & Hartmann, 2012). The GCM-diagnosed feedbacks exhibit considerable spatial and intermodel variability (Colman & Hanson, 2017; Feldl & Bordoni, 2016; Po-Chedley et al., 2018). The tropics and subtropics, where OLR is particularly sensitive to radiatively forced tropospheric changes, correspondingly have large positive water vapor and negative lapse rate feedback parameters. Over the Southern Ocean, where the troposphere is decoupled from the surface response and where surface warming is muted, these feedback parameters vary widely among models (Po-Chedley et al., 2018). To date, no complete theory exists for predicting these feedbacks, though some progress has been recently made in a gray radiation aquaplanet. In that model, an assumption of moist-adiabatic warming yields good estimates of temperature feedback structure across a wide range of climates (Merlis et al., 2022). This approach seeks to bridge the gap between single-column (Koll & Cronin, 2018; Koll et al., 2023; McKim et al., 2021) and local feedback perspectives—both of which emphasize the physical connection between radiative flux at the top of the atmosphere and local surface warming—and is the course of the present study.

A theory of radiative feedbacks is incomplete if it is limited to longwave feedbacks and tropical processes. Though polar feedbacks contribute modestly to the global feedback, their regional contributions are large, and they too are amenable to analytical formulation. Surface albedo and lapse rate feedbacks are the dominant contributors to polar amplification (Goosse et al., 2018; Hahn et al., 2021; Pithan & Mauritsen, 2014). The surface albedo feedback has long been incorporated in simple climate models via a temperature-dependent surface albedo (Budyko, 1969; Feldl & Merlis, 2021; Merlis, 2014; North, 1975; North et al., 1981; Sellers, 1969; Wagner & Eisenman, 2015). The lapse rate feedback is positive in polar regions due to a stably stratified atmosphere that warms more near the surface than aloft, reducing radiative cooling to space relative to vertically uniform warming, especially in winter and in regions of sea-ice retreat (Boeke et al., 2021; Feldl et al., 2020; Jenkins & Dai, 2021). The Arctic atmosphere is thus characterized by a state of radiative-advective equilibrium (Payne et al., 2015) for much of the year (Miyawaki et al., 2022). This balance can be used as a model for polar temperature profiles, with the resulting lapse rate feedback exhibiting sensitivity to the nature of the climate forcing, be it surface, atmospheric, or radiative (Cronin & Jansen, 2016).

These expressions for Earth's regional climate—moist-adiabatic temperature, radiative-advective temperature, and surface albedo—rely on surface temperature. Hence, we ask, how accurately can feedbacks in comprehensive GCMs be approximated given the limited information of surface temperature change only? An analytical model for local radiative feedbacks may seem to be out of reach. The moist adiabatic response to surface warming is known to overpredict the temperature response aloft, due to the influence of large-scale atmospheric circulation, CO_2 radiative forcing, and convective entrainment (Bao et al., 2021; Keil et al., 2021; Miyawaki et al., 2020; Po-Chedley et al., 2019; Wang & Huang, 2021). Radiative-advective temperatures prescribed with fixed atmospheric energy transport neglect the remote influences of changes in energy transport on the polar atmosphere (Henry et al., 2021). Yet, the advantage of these idealizations is that they are grounded in theory and, when convolved with radiative kernels, provide an approximation of the spatially varying Planck, lapse rate, water vapor, and surface albedo feedbacks.

Here, we seek to quantify the contributions of local moist-adiabatic processes to the ensemble mean and intermodel spread in zonal-mean feedbacks; to validate radiative-advective equilibrium as a model for seasonal variations in the polar lapse rate feedback; and to assess the relationship between global-mean analytical feedbacks and GCM-diagnosed feedbacks—for all radiative feedbacks excepting clouds. We regard our predicted feedbacks as "semi-analytical": integrals that appear in the closed-form expressions of the model are evaluated numerically, and radiative kernels, derived from an offline run of the GCM radiation code, are used. We find an impressive degree of agreement given the simplicity of the approach, and the small discrepancies provide a valuable insight into the role of those processes we do not represent.

2. Methods

We present the results of radiative feedbacks computed from the radiative kernel method (Section 2.3) with the changes in radiatively active variables (e.g., temperature, water vapor, or surface albedo) taken diagnostically

from Coupled Model Intercomparison Project (CMIP6) GCM output (Section 2.1) or from the analytical model (Section 2.2) given the GCM-simulated surface temperature change and base-state surface temperature and relative humidity (RH).

2.1. GCM Data

Monthly mean output from 35 models, listed in the legend of Figure 4, from phase 6 of the CMIP6 is used in this study. To calculate radiative feedbacks, climate anomalies are taken as the difference between the piControl and abrupt 4×CO_2 simulations, averaged over years 120–150 for both scenarios. Likewise, climatologies defined by these years provide the surface temperature and pre-industrial RH that are the input to the analytical model, described next.

2.2. Analytical Model

The analytical model includes three components, all driven by near-surface air temperature from the CMIP6 simulations.

Moist adiabatic atmospheric temperature is calculated at each pressure p, latitude ϕ, longitude Λ, and month t. The initial condition of the rising air parcel is given by the near-surface air temperature and RH, with the latter diagnosed from control simulations only; qualitatively similar results are achieved by assuming a uniform 80% near-surface RH, as we will show. Below the lifting condensation level (LCL), we use the dry adiabatic temperature, $\theta(p/p_0)^{R_d/c_p}$, where θ is the potential temperature, p is the atmospheric pressure, p_0 = 1,000 hPa is the reference pressure, R_d = 287.04 J kg^{-1} K^{-1} is the gas constant for dry air, and c_p = 1,006.04 J kg^{-1} K^{-1} is the specific heat of dry air at constant pressure. The temperature and pressure of the LCL are calculated following Romps (2017). Combining Equation 7 of Romps (2016) with the hydrostatic equation and ideal gas law, the lapse rate in pressure coordinates of a dilute moist adiabat can be written:

$$\frac{\partial T_{\mathrm{ma}}}{\partial p} = \frac{1}{p}\frac{(1+a)R_d T + Lq^*}{(1+a)c_p + (L^2 q^*)/(R_v T^2)},$$

where $a = 0.2$ (as suggested by Romps (2016)) is a non-dimensional parameter that increases with entrainment rate ($a = 0$ is an undilute moist adiabat), q^* is the saturation specific humidity, $L = 2.5 \times 10^6$ J kg^{-1} is the latent heat of vapourization, and R_v = 461 J kg^{-1} K^{-1} is the gas constant for water vapor. We then numerically integrate the moist adiabatic lapse rate from the LCL upwards to obtain $T_{\mathrm{ma}}(p, \phi, \Lambda, t)$. Strictly, due to this integration, the model is semi-analytical.

Radiative-advective atmospheric temperature is calculated at each pressure, latitude, longitude, and month. It is derived from the two-stream Schwarzchild equations for windowed-gray infrared radiative transfer, following Cronin and Jansen (2016):

$$T_{\mathrm{ra}}(p, \phi, \Lambda, t) = \left[\frac{\left(F_s + F_a - \beta\sigma T_s^4\right)(1+\tau(p)) + \frac{F_a b}{\tau_0}\left(\frac{\tau(p)}{\tau_0}\right)^{b-1} - \frac{F_a \tau_0}{b+1}\left(\frac{\tau(p)}{\tau_0}\right)^{b+1}}{2\sigma(1-\beta)}\right]^{1/4},$$

where optical thickness τ follows a power law, $\tau = \tau_0(p/p_0)^2$, and surface forcing F_s is a function of surface temperature T_s, $F_s = \left[\sigma T_s^4(2+\beta\tau_0) - F_a\left(1 + \frac{b\tau_0}{b+1}\right)\right](2+\beta\tau_0)^{-1}$. Model parameters for atmospheric moist static energy flux convergence plus solar atmospheric heating, atmospheric window width, total optical thickness, and vertical distribution of heating are tuned to the CMIP6 piControl Arctic wintertime conditions, yielding values of F_a = 150 W m^{-2}, $\beta = 0.2$, $\tau_0 = 4.5$, and $b = 1$, respectively. When and where surface temperatures are less than the critical temperature of −4°C, radiative-advective temperatures are used in the feedback calculations, and elsewhere, moist adiabatic temperatures. The transition between the two regimes is discontinuous. The incorporation of radiative-advective equilibrium distinguishes our approach from other recent studies that compute spatial patterns of feedbacks based on locally moist adiabatic conditions (Koll et al., 2023; Merlis et al., 2022). We emphasize that horizontal atmospheric energy transport is assumed to be constant, and non-local surface warming cannot influence the temperature structure.

Surface albedo is calculated for each latitude, longitude, and month. We use the following form of temperature-dependent surface albedo

$$\alpha(\phi, \Lambda, t) = \frac{\alpha_o + \alpha_i}{2} + \frac{\alpha_o - \alpha_i}{2} \tanh \frac{T_s - T_0}{h_T}.$$

with width parameter $h_T = 2$ K (Merlis, 2014). Model parameters for ocean and ice albedo, and the transition between them, are tuned to CMIP6 piControl conditions, yielding values of $\alpha_o = 0.1$, $\alpha_i = 0.8$, and $T_0 = -4$°C. The critical temperature T_0 determined here is also used for the transition to radiative-advective equilibrium. In the annual mean, the high-latitude regime covers on average 12% of the Earth's surface, with values ranging from 9.0% to 15.8% based on individual CMIP6 models.

2.3. Feedback Analysis

All-sky radiative feedbacks are calculated using the radiative kernel method (Shell et al., 2008; Soden et al., 2008) with the CESM-CAM5 radiative kernel (Pendergrass et al., 2018). We present results of two definitions, local radiative feedbacks and the global-mean of global radiative feedbacks,

$$\lambda_{i,\mathrm{loc}}(\phi, \Lambda, t) = \{K_i \Delta x_i\} \frac{1}{\Delta T_s(\phi)}$$

$$\lambda_{i,\mathrm{glob}} = \left\langle \{K_i \Delta x_i\} \frac{1}{\langle \Delta T_s \rangle} \right\rangle,$$

both in units W m^2 K^{-1}, which differ in whether the radiative response is normalized by the zonal-mean, annual-mean near-surface temperature change or the global-mean, annual-mean near-surface temperature change. As a consequence of this difference in normalization, the global feedback is not equivalent to the global-mean of the local feedback ($\lambda_{\mathrm{glob}} \neq \langle \lambda_{\mathrm{loc}} \rangle$). K is the all-sky radiative kernel (i.e., sensitivity of top-of-atmosphere radiative flux to small perturbations in temperature, water vapor, and surface albedo), Δx is the climate anomaly (e.g., forced change in temperature, water vapor, surface albedo), index $(\cdot)_i$ indicates an individual feedback, $\{\cdot\}$ indicates a tropospheric integral, and $\langle \cdot \rangle$ is a global mean. See Feldl and Roe (2013) and Hedemann et al. (2022) for discussion of feedback definitions. The change in a given state variable Δx is either diagnosed directly from the GCM output or approximated by our analytical model.

Furthermore, we consider both the conventional and RH feedback frameworks. Generally speaking, in the conventional framework (Shell et al., 2008; Soden et al., 2008), the water vapor feedback λ_{wv} is calculated from the change in specific humidity, and the Planck λ_{p} and lapse rate λ_{lr} feedbacks include only the radiative response to temperature change. In the RH-based framework (denoted with $\tilde{\lambda}$, Held & Shell, 2012), the RH feedback $\tilde{\lambda}_{\mathrm{rh}}$ is calculated from the change in RH, and the changes in specific humidity at fixed RH are included with their respective temperature feedback. That is, the fixed-RH Planck feedback $\tilde{\lambda}_{\mathrm{p}}$ includes the moistening associated with vertically uniform warming, and the fixed-RH lapse rate feedback $\tilde{\lambda}_{\mathrm{lr}}$ includes the moistening associated with deviations from vertically uniform warming. By construction, the sum of the conventional feedbacks equals the sum of the RH-based feedbacks. For the analytical model, we do not need to explicitly calculate the change in specific humidity because we assume fixed RH; as is standard, the specific humidity kernel gives the sensitivity of specific humidity to warming at fixed RH (units of W m^2 K^{-1}) (Soden et al., 2008). Therefore, the radiative response to specific humidity changes, used in the calculation of analytical λ_{wv}, $\tilde{\lambda}_{\mathrm{p}}$, and $\tilde{\lambda}_{\mathrm{lr}}$, is given by $\{K_q \Delta T\}$. As will be shown, the intermodel spread is greatly reduced in the RH-based framework, and hence where individual ensemble members are presented, we will focus on that framework.

3. Results

Our analytical model produces local radiative feedbacks that, in the zonal average, strongly resemble feedbacks diagnosed from CMIP6 (Figure 1). This is despite the fact that the analytical feedbacks are computed from thermodynamic arguments, given only the surface temperature change in each CMIP6 model, while the GCM-diagnosed feedbacks depend on the detailed information of the simulated atmospheric and cryospheric response, which includes dynamical influences. In Section 2.2, we present theoretically based expressions for atmospheric temperature and surface albedo, assume fixed RH, and apply the polar regime (to both the surface

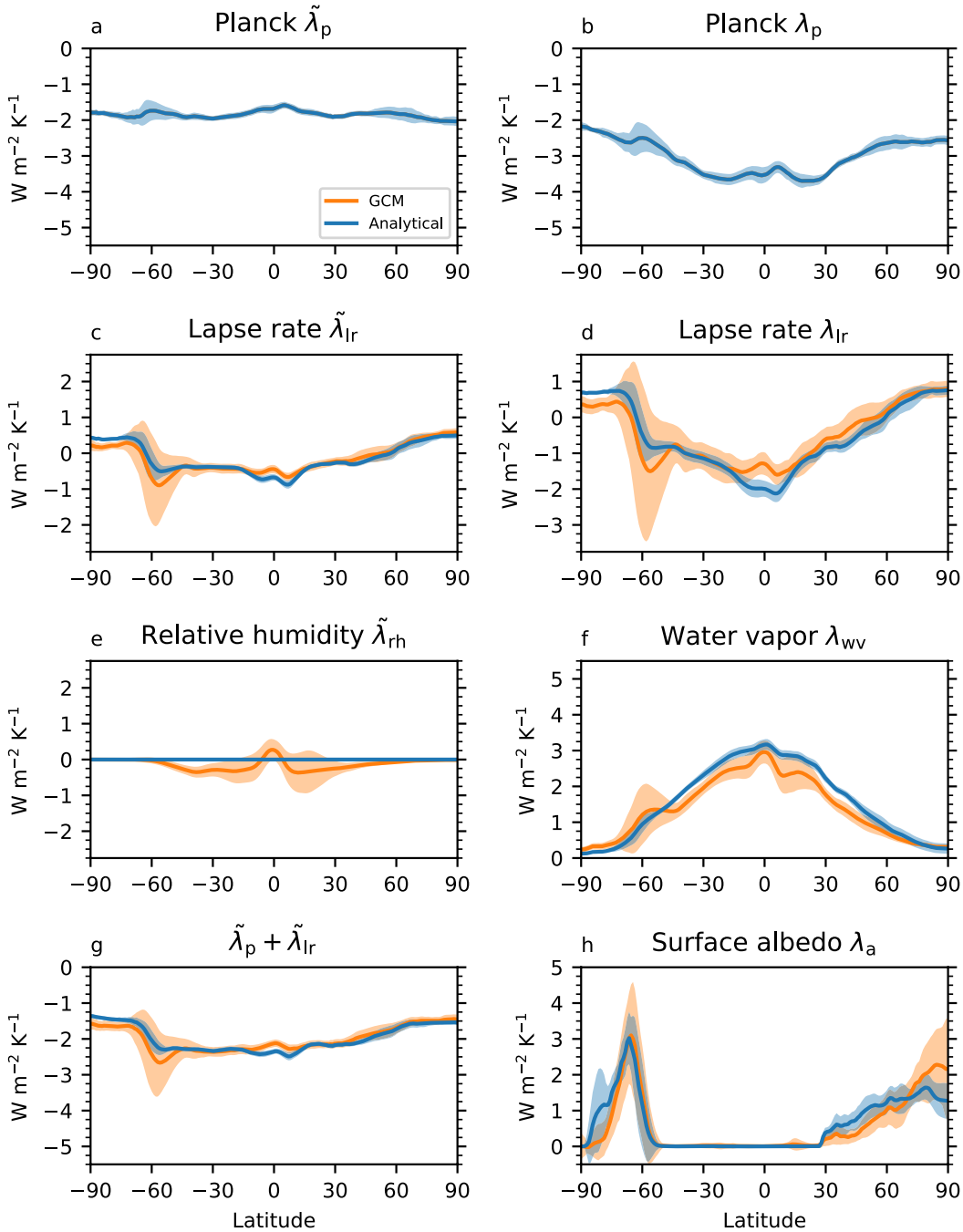

Figure 1. Zonal-mean, annual-mean radiative feedbacks diagnosed from the full general circulation model output including detailed information of the simulated atmospheric and cryospheric response (orange) and estimated analytically given only, for projected changes, the surface temperature response in each Coupled Model Intercomparison Project model (blue). Climate responses used in the feedback calculations are computed from the difference between the piControl and abrupt $4\times CO_2$ simulations, and feedbacks are locally defined. The solid line is the ensemble mean, and the shaded envelope is two standard deviations. The *y*-axis range is the same to facilitate comparison among panels. *Left* Feedbacks are presented following the relative humidity framework, in which temperature feedbacks include the fixed-RH specific humidity changes associated with the component temperature changes (Held & Shell, 2012). *Right* Conventional Planck, lapse rate, water vapor, and surface albedo feedbacks.

albedo and atmospheric temperature) where surface temperatures are less than −4°C. In Figure 1, the resulting analytical Planck feedback is identical by construction to the GCM-diagnosed Planck feedback and describes the effects of vertically uniform warming, as determined by the spatially varying surface temperature change. We present both the fixed-RH $\tilde{\lambda}_p$ and the conventional λ_p; the former combines the warming and, for fixed RH, the moistening concomitant with that warming (Held & Shell, 2012), whereas the latter separates all moistening into a water vapor feedback.

The analytical lapse rate feedback, like the GCM-diagnosed lapse rate feedback, is negative in the tropics and, notably, positive in the polar regions (Figures 1c and 1d). A positive high-latitude lapse rate feedback is a consequence of our representation of radiative-advective equilibrium in the analytical model. In the absence of this process, that is, for purely moist adiabatic warming, the lapse rate feedback is near-zero at high latitudes (Figure S1 in Supporting Information S1). The fixed-RH $\tilde{\lambda}_{lr}$ has a smaller magnitude than the conventional λ_{lr} due to the compensating effects of warming and moistening that are separated in the λ_{lr} and λ_{wv} feedbacks (Figures 1d and 1f). Assuming a uniform near-surface RH of 80%, rather than spatially and seasonally varying RH from pre-industrial control simulations, augments these compensating biases in the lapse rate and water vapor feedbacks but does not qualitatively change the results (Figure S1 in Supporting Information S1). Though we opt to account for entrainment via a scaling factor (Section 2.2), the alternative assumption of an undilute moist adiabat produces only subtle differences in the magnitude of the lapse rate feedback at low latitudes (Figure S1 in Supporting Information S1), which we will further document below for the global-mean net fixed-RH feedback. The analytical model assumes no changes in RH—there is no comprehensive theory for how RH should change—and hence zero RH feedback, and the GCM-diagnosed $\tilde{\lambda}_{rh}$ is small (Figure 1e). Our successful prediction of both the positive high-latitude lapse rate feedback (Figures 1c and 1d) and the surface albedo feedback (Figure 1h) demonstrates that the analytical model characterizes the crucial feedbacks contributing to annual-mean polar amplification, a distinguishing contribution of this study.

The intermodel spread in the analytical feedbacks is reduced compared to the GCM-diagnosed feedbacks. This is true for the individual feedbacks and still holds, though to a slightly lesser degree, for the net fixed-RH feedback ($\tilde{\lambda}_p + \tilde{\lambda}_{lr}$, Figure 1g). The greatest uncertainty originates from the Southern Ocean, where surface temperature change is muted, and is particularly large in the GCM-diagnosed lapse rate feedback (Figures 1c and 1d). The closer intermodel agreement in the analytical lapse rate feedback occurs because the analytical model is strictly coupled to local surface temperature changes, and nonlocal effects on atmospheric temperatures that would increase spread are neglected. This result is consistent with Po-Chedley et al. (2018), which attributes the pronounced intermodel spread in the GCM-diagnosed lapse rate feedback to the nonlocal influence of tropical warming on the extratropical stratification over the Southern Ocean. In other words, the analytical model is a very good predictor of the ensemble-mean, zonal-mean feedback, but nonlocal effects make important contributions to regional uncertainty, particularly in the Southern extratropics. Differences in some CMIP6 model physics will further contribute to spread in the GCM-diagnosed feedbacks but not the analytical feedbacks, presuming they are atmospheric and not surface-based in origin. The meridional structures of intermodel standard deviations are also presented in Figure S2 in Supporting Information S1, which additionally highlights the minimal spread for the fixed-RH analytical feedbacks, $\tilde{\lambda}_p$ and $\tilde{\lambda}_{lr}$, and the substantial spread for the surface albedo feedback.

The success of the analytical model in the zonal mean, particularly for the ensemble-mean feedbacks, prompts the question of whether the seasonal and geographic patterns are also captured with fidelity. Here we focus on the conventional Planck, lapse rate, and water vapor feedbacks in order to highlight the separate effects of temperature and water vapor and, crucially, the separate effects of moist-adiabatic and radiative-advective regimes on the lapse rate feedback. Starting with the seasonal cycle of feedbacks, a small negative bias in the analytical λ_{lr} and a small positive bias in the λ_{wv} (Figure 2) is consistent with tropical upper-tropospheric warming that is greater for the analytical model than GCMs (not shown). The bias is even smaller in $\tilde{\lambda}_{lr}$ (Figure 1). The seasonally varying sea-ice edge is plainly evident as the transition from positive to negative λ_{lr} and as the maxima in λ_a. In particular, the analytical model captures the wintertime positive lapse rate feedback in the Arctic.

The analytical model also broadly reproduces the geographic features of the feedbacks, with a few exceptions. Biases in the analytical λ_{lr} and λ_{wv} are enhanced over land, with continental regions exhibiting stronger respective negative and positive feedbacks in the analytical model (Figures 3c–3f). We speculate this behavior is related to our assumption of constant near-surface RH in the analytical model; decreases in near-surface RH would raise the LCL and reduce warming and moistening aloft. Additional differences in the spatial structure of these feedbacks

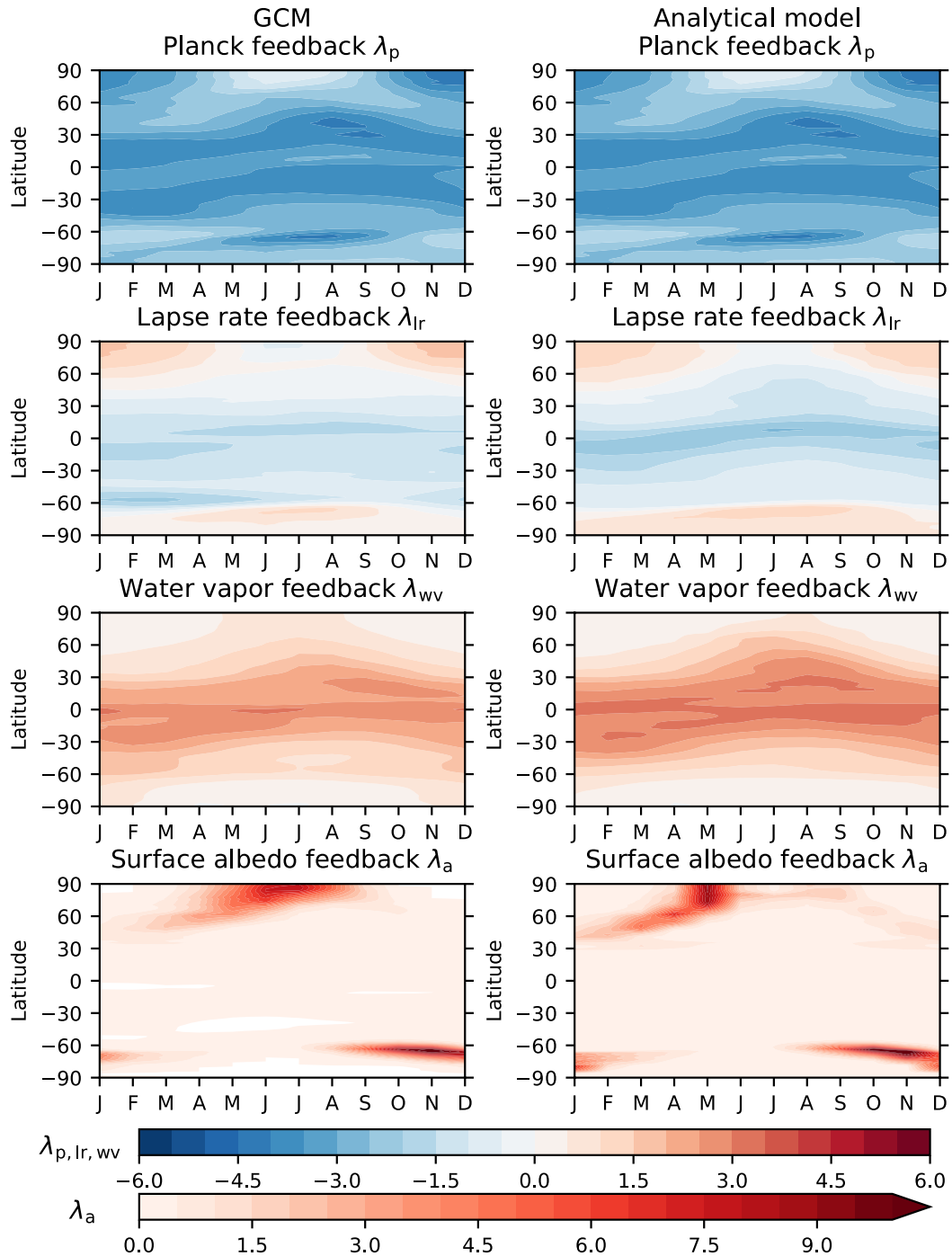

Figure 2. Zonal-mean, ensemble-mean seasonal radiative feedbacks (left) diagnosed from the full general circulation model output and (right) estimated analytically. Feedbacks are locally defined, and they are presented following the conventional framework to emphasize the meridional and seasonal structure of the lapse rate feedback.

are apparent over the East Pacific and Southern Ocean. Specifically, the GCM-diagnosed λ_{lr} is characterized by a tri-pole pattern (Figure 3c), whereas the analytical λ_{lr} is weak in the southeast Pacific and Southern Ocean (Figure 3d). The differences persist in the fixed-RH $\tilde{\lambda}_{lr}$, albeit at weaker magnitude, (not shown) indicating that they are at most only partially compensated by the water vapor feedback. These regions are likely influenced in the GCMs by non-local warming that leads to deviations from an adiabat not characterized by the analytical model. The analytical surface albedo feedback is more positive over continents in both hemispheres (Figures 3g

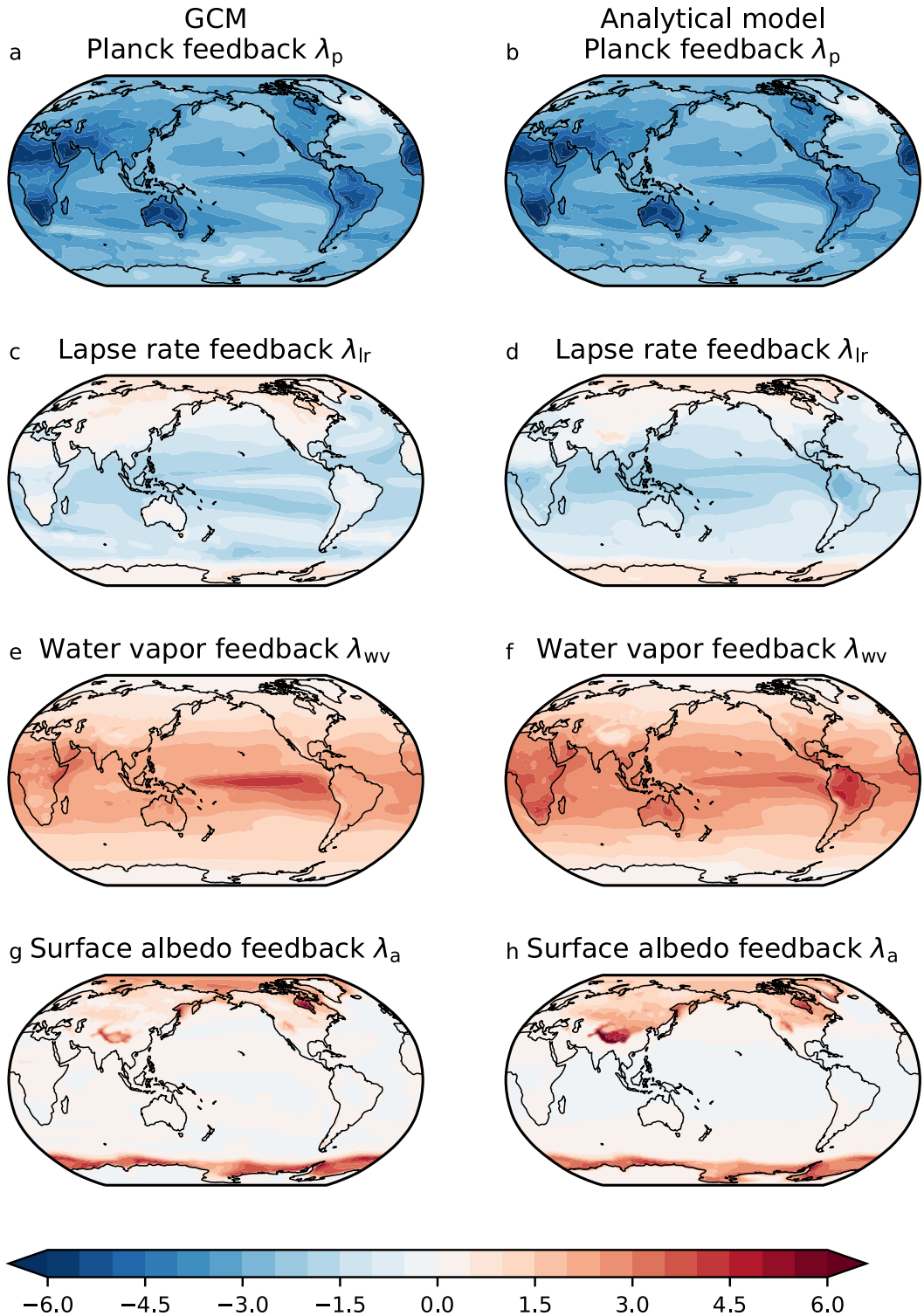

Figure 3. Annual-mean, ensemble-mean radiative feedbacks (left) diagnosed from the full general circulation model output and (right) estimated analytically. Feedbacks are locally defined, and they are presented following the conventional framework.

and 3h), as anticipated from Figure 1h, because the albedo parametrization translates surface warming near the critical temperature into albedo change, whereas glaciated regions in GCMs may change albedo more slowly (due to slower melt rates) or not at all (for static land surface types).

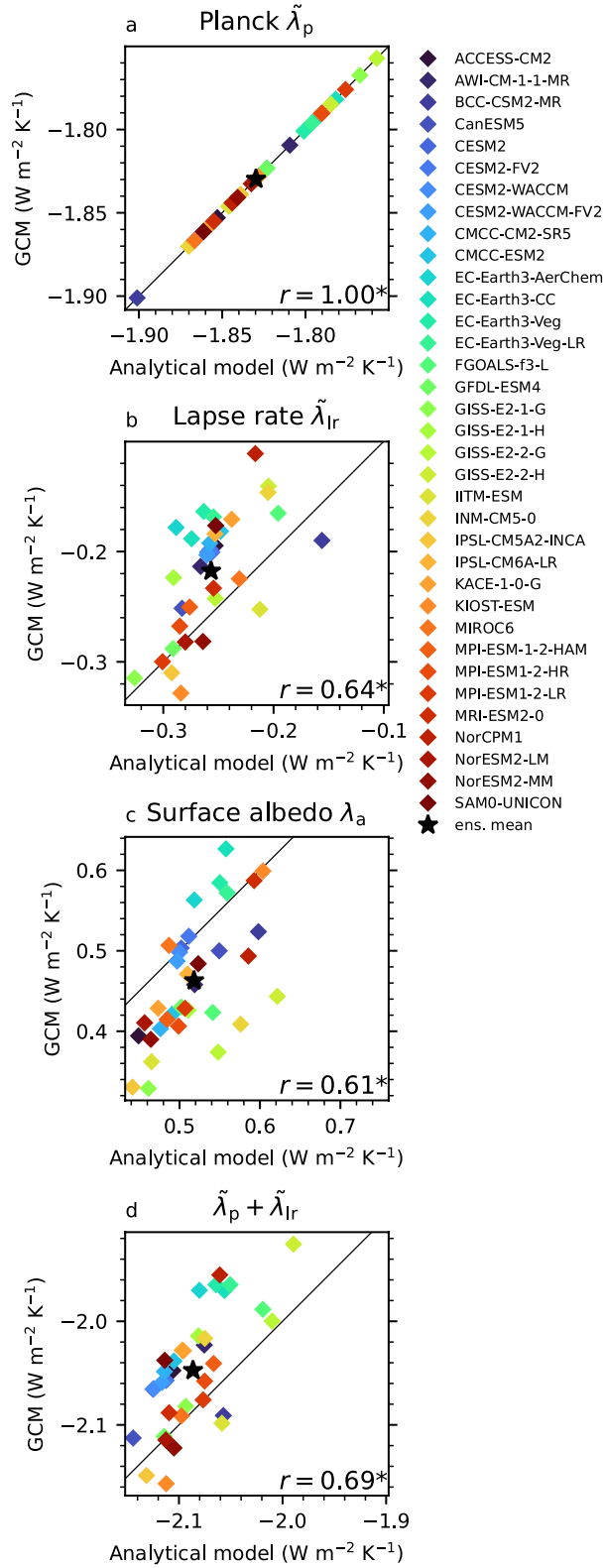

Figure 4. Relationship between global feedbacks diagnosed from general circulation models and estimated analytically. Feedbacks are presented following the relative humidity framework. The 1:1 line is shown for reference. The correlation r is displayed on each plot, and (*) denotes significant correlations at the 1% level. The ensemble mean is indicated by a star.

We next assess the ability of our analytical model to predict global feedbacks, that is, global-mean feedbacks in which the radiative flux change is normalized by the global-mean near-surface temperature change (Section 2.3). Here, we focus on the RH framework for consistency with CMIP6 standards (Zelinka et al., 2020) and to avoid unphysically inflating the intermodel spread. Globally, analytical feedbacks are significantly ($p < 0.01$) correlated with GCM-diagnosed feedbacks across the model ensemble: $r = 0.64$ for the fixed-RH lapse rate feedback $\tilde{\lambda}_{\mathrm{lr}}$, $r = 0.61$ for surface albedo feedback, and $r = 0.69$ for the net fixed-RH feedback (Figure 4). As noted above, the analytical and GCM-diagnosed Planck feedbacks are identical by construction as they rely on the same surface temperature change, applied uniformly through the height of the atmosphere. The ensemble-mean global net fixed-RH feedback estimated from the analytical model is -2.09 W m^{-2} K^{-1} (Figure 4d). For the sensitivity tests described above, this value may be compared to a more stabilizing feedback of -2.24 W m^2 K^{-1} for the purely moist adiabatic case (no radiative-advective equilibrium) and -2.12 W m^2 K^{-1} for the undilute ($a = 0$) case. Hence, high-latitude processes and entrainment both have a weakening effect on the feedback parameter, implying a higher climate sensitivity. In particular, including the radiative-advective energetic regime substantially impacts both regional and global feedbacks. The destabilizing effect of entrainment, which is modest in our results, has also been noted by Bao et al. (2021) for the tropical clear-sky longwave feedback.

Beyond demonstrating the strength of the relationship between analytical and GCM-diagnosed feedbacks, Figure 4 also shows that the analytical global feedbacks are less dispersed than their GCM-diagnosed counterparts, as expected from examining the zonal mean (Figure 1 and Figure S2 in Supporting Information S1). The analytical model slightly underpredicts $\tilde{\lambda}_{\mathrm{lr}}$ and overpredicts λ_{a}—models tend to fall to the left and right of the 1:1 line in Figures 4b and 4c, respectively. The magnitudes of the global-mean net fixed-RH feedback estimated from the analytical model and diagnosed from GCMs agree very well, with ensemble-mean values of -2.09 and -2.05 W m^{-2} K^{-1}, respectively. The GCM-diagnosed net temperature and water vapor feedback (including the RH feedback) is -2.20 W m^{-2} K^{-1}. For the global-mean surface albedo feedback, the analytical and GCM-diagnosed values are 0.52 and 0.46 W m^{-2} K^{-1}, respectively. We emphasize that the net fixed-RH feedback is not equivalent to the longwave clear-sky feedback, which has been a focus of prior theoretical work, because of our use of all-sky radiative kernels that include cloud and shortwave water vapor effects.

4. Conclusions

Radiative feedbacks that govern the Earth's climate sensitivity depend on the atmospheric and cryospheric responses that arise due to a forced surface temperature change. Here, we have quantified the radiative impact of moist adiabatic warming, radiative-advective warming, and a simple ice-albedo feedback on the spatial pattern and intermodel spread in radiative feedbacks. Global feedbacks estimated from the analytical model, which combines thermodynamic theory with radiative kernels, are significantly correlated with GCM-diagnosed feedbacks ($r > 0.6$), predicting a net fixed-RH $\left(\tilde{\lambda}_{\mathrm{p}} + \tilde{\lambda}_{\mathrm{lr}}\right)$ feedback of about -2 W m^{-2} K^{-1} and a surface albedo feedback of about 0.5 W m^{-2} K^{-1}. Regionally, the analytical approximations of atmospheric temperature change produce a lapse rate feedback with remarkably realistic seasonal and meridional variations, including a positive lapse rate feedback in polar regions in months when the atmosphere is in radiative-advective equilibrium and the surface is ice-covered.

This research elucidates the atmospheric warming processes that are of consequence for radiative feedbacks. For the zonal mean and globally, moist-adiabatic warming and radiative-advective warming are necessary and sufficient for characterizing the feedback-relevant warming, and deviations from these theories have little impact. As expected on physical grounds, entrainment has compensating effects on the conventional lapse rate and water vapor feedbacks that are largely canceled in the RH feedback framework. The zonal mean also conceals a mix of overestimated lapse rate feedback over land and underestimated feedback over ocean. We have not identified the processes responsible for this land-ocean bias, though we note that the absence of non-local warming of the upper troposphere would be expected to lead to a less negative rather than a more negative feedback in the analytical model compared to GCMs. Other dilute adiabat formulations, or permitting the analytical model to depend on changes in near-surface RH, may improve the geographical agreement.

The local perspective afforded by the analytical model, when contrasted with the GCM results, reveals additional regions where our idealizations are insufficient to fully explain the feedbacks. Since the radiative flux changes produced by the analytical model are determined by local surface temperature change, they are only influenced by remote regions insofar as circulation changes are implicit in surface temperature changes. Consequently, they

will likely underestimate the pattern effect, that is, the phenomenon that the radiative feedback depends on the uncertain, time-evolving pattern of sea-surface temperature (SST). One source of this time-varying behavior is asserted to originate in the tropical Pacific east-west SST gradient, due to a coupling between lapse rates over the West and East Pacific and low cloud feedbacks over the East Pacific (Andrews & Webb, 2018; Ceppi & Gregory, 2017; Dong et al., 2019, 2021; Zhou et al., 2016). Indeed, we identify the East Pacific as a region with qualitative differences between GCM-diagnosed and analytical feedbacks (Figure 3). Furthermore, the analytical feedbacks presented here feature less intermodel variability overall. Hence, nonlocal effects and a decoupling of the troposphere from the surface response are expected to be an important contributor to the uncertainty in radiative feedbacks, likely explaining in part the differences in intermodel variability between the analytical and GCM-diagnosed feedbacks. Nevertheless, the ensemble-mean feedback, particularly its zonal mean and seasonality, are striking predictions by the analytical model. Future work will investigate the sensitivity of the analytical feedbacks to other patterns of surface warming beyond the abrupt $4\times CO_2$ scenario. Additionally, though here we treat the advection-dependence of radiative-advective temperature (F_a) as constant, this term could instead scale with the meridional temperature or energy gradients to represent changes in atmospheric energy transport. However, as currently configured, the analytical temperature and water vapor feedbacks are in close agreement with those diagnosed from GCMs at high latitudes.

The analytical model, which we have used to predict feedbacks in future warm climates, provides a foundation for understanding regional, seasonal, and intermodel variations in radiative feedbacks from simple physics. The atmospheric and cryospheric responses emerge from the spatial pattern of surface temperature change, which we base on GCM projections though in principle they are not reliant on running a GCM. By implication, radiative feedbacks may be similarly estimated for past or present climates, given observed or proxy-based surface temperature changes.

Data Availability Statement

Data supporting this research is freely available from the Earth System Grid Federation (https://esgf-node.llnl.gov/search/cmip6/) for the 35 CMIP6 models listed in the legend of Figure 4. The CAM5 radiative kernels are available at Pendergrass (2017).

Acknowledgments
This material is based upon work supported by the National Science Foundation under Award AGS-1753034 (NF) and the Cooperative Institute for Modelling Earth Systems under award NA18OAR4320123 from the National Oceanic and Atmospheric Administration, U.S. Department of Commerce (TMM). We thank Isaac Held and Nadir Jeevanjee for helpful discussions. We also acknowledge the World Climate Research Programme, which, through its Working Group on Coupled Modelling, coordinated and promoted CMIP6. We thank the climate modeling groups for producing and making available their model output, the Earth System Grid Federation (ESGF) for archiving the data and providing access, and the multiple funding agencies who support CMIP6 and ESGF.

References

Andrews, T., & Webb, M. J. (2018). The dependence of global cloud and lapse rate feedbacks on the spatial structure of tropical Pacific warming. *Journal of Climate*, *31*(2), 641–654. https://doi.org/10.1175/JCLI-D-17-0087.1

Bao, J., Stevens, B., Kluft, L., & Jiménez-de-la Cuesta, D. (2021). Changes in the tropical lapse rate due to entrainment and their impact on climate sensitivity. *Geophysical Research Letters*, *48*(18), e2021GL094969. https://doi.org/10.1029/2021GL094969

Boeke, R. C., Taylor, P. C., & Sejas, S. A. (2021). On the nature of the Arctic's positive lapse-rate feedback. *Geophysical Research Letters*, *48*(1), e2020GL091109. https://doi.org/10.1029/2020GL091109

Budyko, M. I. (1969). The effect of solar radiation variations on the climate of the Earth. *Tellus*, *21*(5), 611–619. https://doi.org/10.3402/tellusa.v21i5.10109

Ceppi, P., & Gregory, J. M. (2017). Relationship of tropospheric stability to climate sensitivity and Earth's observed radiation budget. *Proceedings of the National Academy of Sciences of the United States of America*, *114*(50), 13126–13131. https://doi.org/10.1073/pnas.1714308114

Chung, E. S., Yeomans, D., & Soden, B. J. (2010). An assessment of climate feedback processes using satellite observations of clear-sky OLR. *Geophysical Research Letters*, *37*(2), L02702. https://doi.org/10.1029/2009GL041889

Colman, R., & Hanson, L. (2017). On the relative strength of radiative feedbacks under climate variability and change. *Climate Dynamics*, *49*(5–6), 2115–2129. https://doi.org/10.1007/S00382-016-3441-8/FIGURES/8

Cronin, T. W., & Jansen, M. F. (2016). Analytic radiative-advective equilibrium as a model for high-latitude climate. *Geophysical Research Letters*, *43*(1), 449–457. https://doi.org/10.1002/2015GL067172

Dessler, A. E., Yang, P., Lee, J., Solbrig, J., Zhang, Z., & Minschwaner, K. (2008). An analysis of the dependence of clear-sky top-of-atmosphere outgoing longwave radiation on atmospheric temperature and water vapor. *Journal of Geophysical Research*, *113*(D17), 17102. https://doi.org/10.1029/2008JD010137

Dong, Y., Armour, K. C., Proistosescu, C., Andrews, T., Battisti, D. S., Forster, P. M., et al. (2021). Biased estimates of equilibrium climate sensitivity and transient climate response derived from historical CMIP6 simulations. *Geophysical Research Letters*, *48*(24), e2021GL095778. https://doi.org/10.1029/2021GL095778

Dong, Y., Proistosescu, C., Armour, K. C., & Battisti, D. S. (2019). Attributing historical and future evolution of radiative feedbacks to regional warming patterns using a Green's function approach: The Preeminence of the western Pacific. *Journal of Climate*, *32*(17), 5471–5491. https://doi.org/10.1175/JCLI-D-18-0843.1

Feldl, N., & Bordoni, S. (2016). Characterizing the Hadley circulation response through regional climate feedbacks. *Journal of Climate*, *29*(2), 613–622. https://doi.org/10.1175/JCLI-D-15-0424.1

Feldl, N., & Merlis, T. M. (2021). Polar amplification in idealized climates: The role of ice, moisture, and seasons. *Geophysical Research Letters*, *48*(17), e2021GL094130. https://doi.org/10.1029/2021GL094130

Feldl, N., Po-Chedley, S., Singh, H. K., Hay, S., & Kushner, P. J. (2020). Sea ice and atmospheric circulation shape the high-latitude lapse rate feedback. *npj Climate and Atmospheric Science*, *3*(1), 41. https://doi.org/10.1038/s41612-020-00146-7

Feldl, N., & Roe, G. H. (2013). Four perspectives on climate feedbacks. *Geophysical Research Letters*, *40*(15), 4007–4011. https://doi.org/10.1002/grl.50711

Feng, J., Paynter, D., & Menzel, R. (2023). How a stable greenhouse effect on Earth is maintained under global warming. *Journal of Geophysical Research: Atmospheres*, *128*(9), e2022JD038124. https://doi.org/10.1029/2022JD038124

Goosse, H., Kay, J. E., Armour, K. C., Bodas-Salcedo, A., Chepfer, H., Docquier, D., et al. (2018). Quantifying climate feedbacks in polar regions. *Nature Communications*, *9*(1), 1–13. https://doi.org/10.1038/s41467-018-04173-0

Hahn, L. C., Armour, K. C., Zelinka, M. D., Bitz, C. M., & Donohoe, A. (2021). Contributions to polar amplification in CMIP5 and CMIP6 models. *Frontiers in Earth Science*, *9*, 725. https://doi.org/10.3389/feart.2021.710036

Hedemann, C., Mauritsen, T., Jungclaus, J., & Marotzke, J. (2022). Reconciling conflicting accounts of local radiative feedbacks in climate models. *Journal of Climate*, *35*(10), 3131–3146. https://doi.org/10.1175/JCLI-D-21-0513.1

Held, I. M., & Shell, K. M. (2012). Using relative humidity as a state variable in climate feedback analysis. *Journal of Climate*, *25*(8), 2578–2582. https://doi.org/10.1175/JCLI-D-11-00721.1

Henry, M., Merlis, T. M., Lutsko, N. J., & Rose, B. E. J. (2021). Decomposing the drivers of polar amplification with a single column model. *Journal of Climate*, *34*(6), 2355–2365. https://doi.org/10.1175/jcli-d-20-0178.1

Ingram, W. (2010). A very simple model for the water vapour feedback on climate change. *Quarterly Journal of the Royal Meteorological Society*, *136*(646), 30–40. https://doi.org/10.1002/QJ.546

Jeevanjee, N., Koll, D. D., & Lutsko, N. (2021). "Simpson's Law" and the spectral cancellation of climate feedbacks. *Geophysical Research Letters*, *48*(14), e2021GL093699. https://doi.org/10.1029/2021GL093699

Jenkins, M., & Dai, A. (2021). The impact of sea-ice loss on Arctic climate feedbacks and their role for Arctic amplification. *Geophysical Research Letters*, *48*(15), e2021GL094599. https://doi.org/10.1029/2021GL094599

Keil, P., Schmidt, H., Stevens, B., & Bao, J. (2021). Variations of tropical lapse rates in climate models and their implications for upper-tropospheric warming. *Journal of Climate*, *34*(24), 9747–9761. https://doi.org/10.1175/JCLI-D-21-0196.1

Koll, D. D., & Cronin, T. W. (2018). Earth's outgoing longwave radiation linear due to H_2O greenhouse effect. *Proceedings of the National Academy of Sciences of the United States of America*, *115*(41), 10293–10298. https://doi.org/10.1073/pnas.1809868115

Koll, D. D., Jeevanjee, N., & Lutsko, N. J. (2023). An analytic model for the clear-sky longwave feedback. *Journal of the Atmospheric Sciences*, *80*(8), 1923–1951. https://doi.org/10.1175/JAS-D-22-0178.1

McKim, B. A., Jeevanjee, N., & Vallis, G. K. (2021). Joint dependence of longwave feedback on surface temperature and relative humidity. *Geophysical Research Letters*, *48*(18), e2021GL094074. https://doi.org/10.1029/2021GL094074

Merlis, T. M. (2014). Interacting components of the top-of-atmosphere energy balance affect changes in regional surface temperature. *Geophysical Research Letters*, *41*(20), 7291–7297. https://doi.org/10.1002/2014GL061700

Merlis, T. M., Feldl, N., & Caballero, R. (2022). Changes in poleward atmospheric energy transport over a wide range of climates: Energetic and diffusive perspectives and a priori theories. *Journal of Climate*, *35*(20), 2933–2948. https://doi.org/10.1175/JCLI-D-21-0682.1

Miyawaki, O., Shaw, T. A., & Jansen, M. F. (2022). Quantifying energy balance regimes in the modern climate, their link to lapse rate regimes, and their response to warming. *Journal of Climate*, *35*(3), 1045–1061. https://doi.org/10.1175/JCLI-D-21-0440.1

Miyawaki, O., Tan, Z., Shaw, T. A., & Jansen, M. F. (2020). Quantifying key mechanisms that contribute to the deviation of the tropical warming profile from a moist adiabat. *Geophysical Research Letters*, *47*(20), e2020GL089136. https://doi.org/10.1029/2020GL089136

North, G. R. (1975). Theory of energy-balance climate models. *Journal of the Atmospheric Sciences*, *32*(11), 2033–2043. https://doi.org/10.1175/1520-0469(1975)032⟨2033:TOEBCM⟩2.0.CO;2

North, G. R., Cahalan, R. F., & Coakley, J. A. (1981). Energy balance climate models. *Reviews of Geophysics*, *19*(1), 91–121. https://doi.org/10.1029/RG019i001p00091

Payne, A. E., Jansen, M. F., & Cronin, T. W. (2015). Conceptual model analysis of the influence of temperature feedbacks on polar amplification. *Geophysical Research Letters*, *42*(21), 9561–9570. https://doi.org/10.1002/2015GL065889

Pendergrass, A. G. (2017). CAM5 radiative kernels [Dataset]. https://doi.org/10.5065/D6F47MT6

Pendergrass, A. G., Conley, A., & Vitt, F. M. (2018). Surface and top-of-atmosphere radiative feedback kernels for CESM-CAM5. *Earth System Science Data*, *10*(1), 317–324. https://doi.org/10.5194/essd-10-317-2018

Pithan, F., & Mauritsen, T. (2014). Arctic amplification dominated by temperature feedbacks in contemporary climate models. *Nature Geoscience*, *7*(3), 181–184. https://doi.org/10.1038/ngeo2071

Po-Chedley, S., Armour, K. C., Bitz, C. M., Zelinka, M. D., Santer, B. D., Fu, Q., & Fu, Q. (2018). Sources of intermodel spread in the lapse rate and water vapor feedbacks. *Journal of Climate*, *31*(8), 3187–3206. https://doi.org/10.1175/JCLI-D-17-0674.1

Po-Chedley, S., Zelinka, M. D., Jeevanjee, N., Thorsen, T. J., & Santer, B. D. (2019). Climatology explains intermodel spread in tropical upper tropospheric cloud and relative humidity response to greenhouse warming. *Geophysical Research Letters*, *46*(22), 13399–13409. https://doi.org/10.1029/2019GL084786

Raghuraman, S. P., Paynter, D., & Ramaswamy, V. (2019). Quantifying the drivers of the clear sky greenhouse effect, 2000–2016. *Journal of Geophysical Research: Atmospheres*, *124*(21), 11354–11371. https://doi.org/10.1029/2019JD031017

Raval, A., & Ramanathan, V. (1989). Observational determination of the greenhouse effect. *Nature*, *342*(6251), 758–761. https://doi.org/10.1038/342758a0

Romps, D. M. (2016). Clausius-Clapeyron scaling of CAPE from analytical solutions to RCE. *Journal of the Atmospheric Sciences*, *73*(9), 3719–3737. https://doi.org/10.1175/JAS-D-15-0327.1

Romps, D. M. (2017). Exact expression for the lifting condensation level. *Journal of the Atmospheric Sciences*, *74*(12), 3891–3900. https://doi.org/10.1175/JAS-D-17-0102.1

Sellers, W. D. (1969). A global climatic model based on the energy balance of the Earth-atmosphere system. *Journal of Applied Meteorology*, *8*(3), 392–400. https://doi.org/10.1175/1520-0450(1969)008⟨0392:agcmbo⟩2.0.co;2

Shell, K. M., Kiehl, J. T., & Shields, C. A. (2008). Using the radiative kernel technique to calculate climate feedbacks in NCAR's Community Atmospheric Model. *Journal of Climate*, *21*(10), 2269–2282. https://doi.org/10.1175/2007JCLI2044.1

Simpson, G. C. (1928). Some studies in terrestrial radiation. *Memoirs of the Royal Meteorological Society*, *2*(16), 69–95.

Soden, B. J., Held, I. M., Colman, R., Shell, K. M., Kiehl, J. T., & Shields, C. A. (2008). Quantifying climate feedbacks using radiative kernels. *Journal of Climate*, *21*(14), 3504–3520. https://doi.org/10.1175/2007JCLI2110.1

Wagner, T. J. W., & Eisenman, I. (2015). How climate model complexity influences sea ice stability. *Journal of Climate*, *28*(10), 3998–4014. https://doi.org/10.1175/jcli-d-14-00654.1

Wang, Y., & Huang, Y. (2021). A single-column simulation-based decomposition of the tropical upper-tropospheric warming. *Journal of Climate*, *34*(13), 5337–5348. https://doi.org/10.1175/JCLI-D-20-0726.1

Zelinka, M. D., & Hartmann, D. L. (2012). Climate feedbacks and their implications for poleward energy flux changes in a warming climate. *Journal of Climate*, *25*(2), 608–624. https://doi.org/10.1175/JCLI-D-11-00096.1

Zelinka, M. D., Myers, T. A., McCoy, D. T., Po-Chedley, S., Caldwell, P. M., Ceppi, P., et al. (2020). Causes of higher climate sensitivity in CMIP6 models. *Geophysical Research Letters*, *47*(1), e2019GL085782. https://doi.org/10.1029/2019GL085782

Zhou, C., Zelinka, M. D., & Klein, S. A. (2016). Impact of decadal cloud variations on the Earth's energy budget. *Nature Geoscience*, *9*(12), 871–874. https://doi.org/10.1038/ngeo2828